Environmental radioactivity and trace metals in surficial sediments from estuarine systems in Ghana (Equatorial Africa), impacted by artisanal gold-mining

Emmanuel Klubi [a], José M. Abril [b,*], Juan Mantero [c], Rafael García-Tenorio [c,d], Elvis Nyarko [a,e]

[a] Department of Marine and Fisheries Sciences, University of Ghana, Legon, Ghana
[b] Departamento de Física Aplicada I. Universidad de Sevilla. ETSIA, Sevilla, Spain
[c] Departamento de Física Aplicada II, Universidad de Sevilla. ETSA, Sevilla, Spain
[d] Centro Nacional Aceleradores (Universidad de Sevilla-Junta Andalucía-CSIC), Sevilla, Spain
[e] Vice Chancellor of the Regional Maritime University, Acra, Ghana

Keywords:
Environmental radioactivity
Volta estuary
Ankobra estuary
Pra estuary
Gold-mining
Heavy metals

A B S T R A C T

This paper reports concentrations of γ-emitter radionuclides (^{40}K, ^{137}Cs, ^{210}Pb, ^{226}Ra, ^{228}Ra, ^{228}Th and ^{234}Th) and some metals (Al, Cr, Fe, Co, Ni, Cu, Zn, As, Sr, Cd, Sb, Cs, Pb, Th and U) in surficial sediments from the Ankobra, Pra and Volta estuaries, in Ghana. Artisanal gold-mining in the Ankobra and Pra basins promoted moderate enrichments of As, Sb, Cu, Cs and Cr in their estuarine sediments, with respect to the reference background of the Volta Estuary. Radionuclide concentrations were in the range found in the Earth's crust. Present data do not support any conclusion on their potential enrichments due to gold-mining activities. Radionuclide isotopic ratios revealed a transfer of ^{228}Ra from sediments to the water column. Pearson correlation coefficient matrices showed different patterns, which were reasonably understood after novel approaches: i) inter-estuaries comparison of slopes in the linear regressions of element-concentrations vs Al, Fe and Cs; ii) study of Al-normalized concentrations of elements; iii) excess ^{210}Pb informing on local sedimentary conditions. The metal enrichments observed in the Ankobra and Pra estuaries are associated with the Fe-rich compounds in sulphide ores (such as FeAsS) transported along the river course and deposited in the estuary.

1. Introduction

Anthropogenic activities are increasingly altering the landscape and affecting sediment fluxes to the aquatic environments. Estuaries are effective sediment traps due to their particular hydrodynamics and they can represent one of the ultimate sinks for pollutants discharged into the aquatic environment.

Measuring concentrations of potentially harmful elements, such as some heavy metals, is in the basis for the environmental risk assessment of the sediment compartment (Tarazona et al., 2014). Sediment quality guidelines (SQGs), based upon the definition of reference toxicity values, can be used for screening purposes (Macdonald et al., 1996). Other pollution indexes, such as the enrichment factor (*EF*) and the geo-accumulation index (I_{geo}) are based upon the comparison with suitable reference levels (Loring and Rantala, 1992). The radionuclide content in sediments can pose radiological hazards, and there are several established indexes for assessing the radiation dose to humans (e.g., Botwe et al., 2017) and to a series of reference organisms (Larsson, 2008).

Multielemental and isotopic analysis, among other sediment properties, can support the sediment fingerprinting technique, allowing for the identification of sediment sources and the understanding of some features of sediment dynamics within river basins (Koiter et al., 2013; Reese et al., 2019). Natural occurring radionuclides have been used for assessing anthropogenic impacts in river basins and estuaries, such as the releases from the phosphate industry (Travesi et al., 1997), the magnitude and impact of acid mining drainage and industrial effluents (Hierro et al., 2012; Villa et al., 2011), or conventional metal mining activities (Manjón et al., 2019).

The study in sediment cores of the ^{210}Pb found in excess with respect to its parent radionuclide, ^{226}Ra, has shown to provide useful insights on the functioning of the sedimentary systems at a centennial time scale

* Corresponding author. Departamento de Física Aplicada I, ETSIA, Universidad de Sevilla, Carretera de Utrera km 1, D.P. 41013, Sevilla, Spain.
E-mail address: jmabril@us.es (J.M. Abril).

(Robbins, 1978; Mabit et al., 2014). Independent chronostratigraphic information can be provided by ^{137}Cs, a man-made radionuclide first introduced in the environment after the atmospheric nuclear weapon tests (Robbins and Edgington, 1975; Sánchez et al., 1992; Abril, 2003; Abril et al., 2018). The radiometric dating of estuarine sediments allows estimating sediment accumulation rates and the reconstruction of temporal records of pollution (e.g., Álvarez-Iglesias et al., 2007; Costa-Böddeker et al., 2018; Sun et al., 2019).

Apart from the radiometric dating, the combined study of radionuclides and trace metals in estuarine sediments is unusual. At present, one of the main limitations of the sediment fingerprinting approach is the non-conservative behaviour of the properties of transported sediments, which limits the sole use of statistical analyses (Koiter et al., 2013). In studies on the spatial distribution of pollutants in surficial estuarine sediments some of the sampling sites may be subject to transient and dynamic sedimentary conditions (e.g., close to areas with sand bars dynamics, recoiling shorelines, or localized entries of terrigenous flows from the banks) involving the continuous and/or episodic reallocation of large amounts of sediments which are carrying a metals load which may be decoupled from the recent pollution history in the estuary. The conclusions of the study could be then biased or limited by the number and distribution of samples with achronological sedimentary conditions. Handling a large number of dated sediment cores is not feasible in many cases, but the measurement of $^{210}Pb_{exc}$ concentrations in surficial sediments can provide some valuable insights on the local sedimentary conditions, as shown in this paper with the support of historical satellite photographs. This can help to a better understanding on the pathways and dynamics of pollution by heavy metals and other hazardous materials. Apart from the obvious radiological interest, including radionuclides in geochemical studies also can contribute, among others, to give insights on varying digestion yields when applying pseudo-total methods and to reinforce the physic-chemical meaning of some statistical correlations.

In Ghana, Equatorial Africa, the Volta Estuary is affected by the anthropogenic fingerprint of the Ada Foah city and by upstream damming, while the Ankobra and Pra estuaries are affected by artisanal gold-mining activities (Donkor et al., 2006; Klubi et al., 2018). The use of Hg for amalgam in small-scale gold mining was legalized in Ghana in 1989, leading to an increase in these activities which nowadays provides employment to over one million people and makes Ghana to account for half of the total gold production in the region. Mercury pollution is then a major threat for environmental and human health. Other major impacts are land degradation and the huge amount of terrigenous inputs injected into the water courses, with mining tailings carrying high concentrations of As, Cr, Zn, Cu and Pb, among other potentially harmful elements (Donkor et al., 2006; Fashola et al., 2016). Thus, Klubi et al. (2018), in their study of these three estuaries, found a moderate to significant contamination of As, Ag and Cu in sediments from the Pra and Ankobra estuaries.

It is known that gold-mining tailings may contain high concentrations of natural radionuclides, as it has been documented in South Africa (Winde and Sandham, 2004). The available data suggest that this is also the case in Ghana (Doyi et al., 2013).

This paper is aimed at studying environmental γ-emitter radionuclides (^{40}K, ^{137}Cs, ^{210}Pb, ^{226}Ra, ^{228}Ra, ^{228}Th and ^{234}Th), along with some major and trace metals (Al, Cr, Fe, Co, Ni, Cu, Zn, As, Sr, Cd, Sb, Cs, Pb, Th and U) in surficial sediments from three estuarine systems (Ankobra, Pra and Volta) in Equatorial Africa. The work focuses on the radionuclide fingerprint of the estuaries, on whether the gold-mining activities in the Ankobra and Pra basins could affect their concentrations, and on some novel aspects of the combined use of the multielemental analysis by ICP-MS and gamma spectrometry for assessing environmental pollution, particularly on the use of $^{210}Pb_{exc}$ as an indicator of local sedimentary conditions. Gamma measurements and some complementary analysis were performed for this work, while for the ICP-MS analytes we use the data generated in the work by Klubi et al. (2018).

2. Materials and methods

2.1. Studied area

Fig. 1 shows satellite images of the three studied estuaries. The Volta River drains about 70% of the Ghana's hydrological basin and has two hydro-dams built on it in 1965 and 1982, respectively. Its estuary forms a delta system, dominated by alluvial sediments and continental clastic sedimentary rocks. Coconut and mangrove dominate the vegetation cover at its peripheries. The Ada community is the largest human settlement in the area.

The Pra and Ankobra estuaries are located in the Ghana's Western Region, which is a tropical rain forest zone. Its geology is associated with

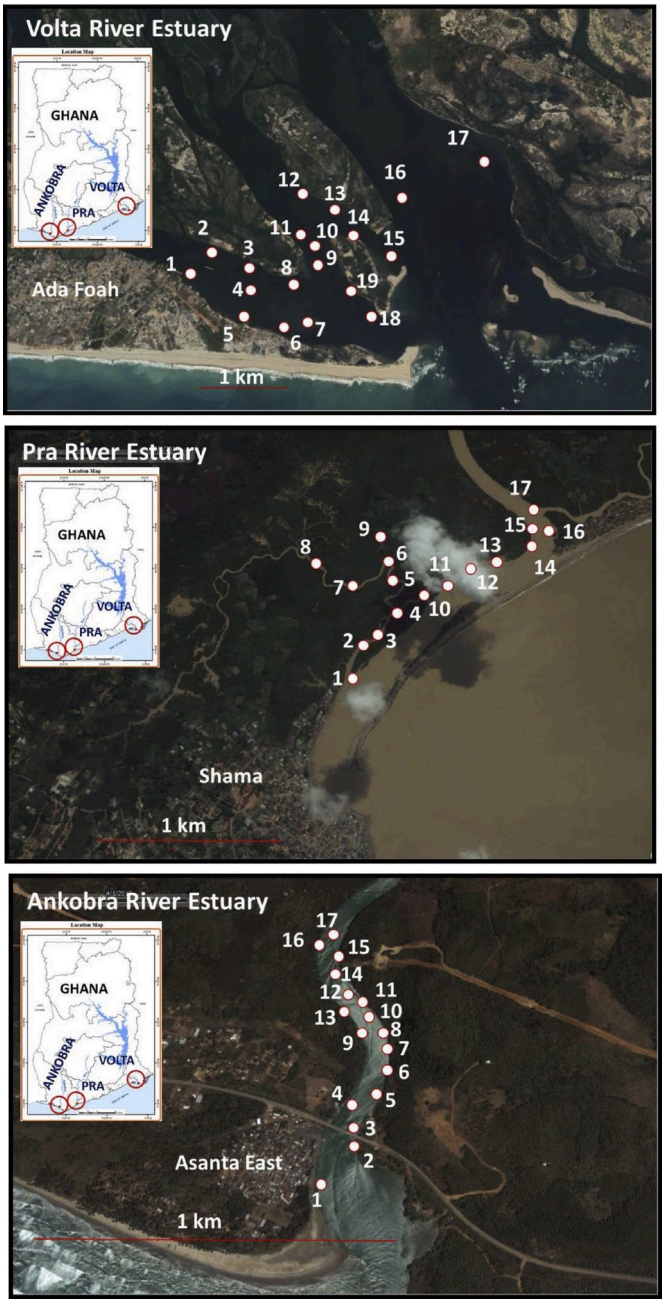

Fig. 1. Satellite images (from Google Earth) of the Volta, Pra and Ankobra estuaries in Ghana (representative for the time of sampling, on early 2017). The locations of the sampling sites of surficial sediments used in this study are depicted.

alluvial gold deposits in basal rock underlying by meta-sedimentary and volcanic of the Biriamian and Tarkwaian systems. In this rural south-western portion of Ghana, the lack of industrial activities makes small-scale gold mining the main source of water resource contamination with potentially toxic elements (Klubi et al., 2018).

The Pra Estuary is located in the eastern side of the Shama Township. It forms a network of multiple channels lying parallel to the coastline with islands mostly flooded during high tides and in the wet season.

The west coastline of the Ankobra Estuary comprises beaches with coconut plants providing defences structure for sand dunes. Axim, Ankobra and Asanta are the largest human settlements in the area. More details on the studied estuaries can be found in Klubi et al. (2018).

The geology of Ghana is described in Petersson et al. (2018). Two types of gold-bearing ores are mined in Ghana: i) quartz vein (quartz with free gold in association with lesser amounts of various metals) and ii) sulphide ores (arsenopyrite) associated with gold, iron, zinc, lead and copper (Nude and FoliYidana, 2011). Bempah et al. (2013) studied tailing dams of gold mines at Obuasi, in the Pra Basin. They reported the texture of tailings being of silty clay loam to clay, with concentrations ranging from 542 to 1752 mg kg^{-1} for As, from 129 to 1848 mg kg^{-1} for Mn, from 24 to 92 mg kg^{-1} for Cu, from 79.5 to 204 mg kg^{-1} for Zn and from 4.1 to 75% for Fe.

2.2. Sampling, sample preparation and characterization (mud and LOI contents)

Surface sediment samples (n = 17–19, of ~0.2 kg d.w. each) were collected from each of the studied estuaries between 27th January and 5th February 2017 by using an Ekman grab (see sampling sites in Fig. 1). Water depths at the sampling sites ranged from 1 to 15 m. The sampling criterion for the Ankobra and Pra estuaries, with a well-defined main channel, was to follow the flow line of the water over a representative area. Sampling in the Pra was complemented along the course of a major tributary flow in its right bank. In the Volta Estuary, with an intricate mesh of channels and islands, the sampling criterion was to cover a representative area around Ada Foah.

Samples were transferred into pre-labelled Ziplock bags, sealed and stored frozen in the Marine and Fisheries' laboratory in the University of Ghana. They were latter thawed, dried at 50 °C using a Gallen Kamp Plus II oven to a constant weight, and re-packaged and transported to the laboratory of environmental radioactivity of the University of Seville, Spain.

Aliquots of each original sediment sample were pre-conditioned by oven-drying overnight at 105 °C, and latter ignited at 440 °C for 3.5 h for determination of loss of ignition (LOI_{440}), given as a percentage of the dry mass. This parameter provides an estimation of the organic matter content in the samples.

The rest of the sample material was gently disaggregated using an agate mortar and then passed through a 2 mm mesh and submitted for analysis. After non-destructive gamma measurements, samples were passed through a sieving column with mesh sizes of 1000, 63 and 25 μm. The fine fraction (particle sizes < 63 μm) is reported as percentage of mass.

2.3. Gamma spectrometry analysis

Samples for gamma measurements were homogenized and sealed in Petri-dishes (76.0 ± 0.5 mL, internal radius 43.3 mm, height 2.9 mm) to prevent escape of ^{222}Rn, and stored long enough to establish secular equilibrium among ^{226}Ra, ^{214}Bi and ^{214}Pb. The Petri dishes were completely filled with sediments, without void spaces, to avoid systematic errors due to radon accumulation at the upmost empty layer; then they were sealed with silicone gel and tape and vacuum packed, following the methodology by Mauring and Gäfvert (2013).

Samples were measured in an extended range Germanium coaxial detector (XtRa) HPGe of 42.1% relative efficiency with 1.95 keV FWHM for ^{60}Co 1332 keV emission and 1.03 keV FWHM for ^{57}Co 0.122 keV emission. Passive shielding is composed of 10 cm Lead (65 ± 3 Bq/kg of ^{210}Pb) internally lined with a 5 mm electrolytic copper layer. Calibration processes in energy, resolution and efficiency were performed following the methodology described in Mantero et al. (2013), by using the IAEA-RGU-1 and IAEA-RGTh-1 reference materials. Self-absorption corrections for low energy emissions (mainly ^{210}Pb and ^{234}Th) have been applied following the procedure described in the above reference.

Activity concentrations of ^{226}Ra were estimated through its progeny radionuclides (^{214}Bi and ^{214}Pb) and reported as the averaged values for their emissions at 609.3 and 1764 keV for ^{214}Bi, and 295 and 351.9 keV for ^{214}Pb. ^{210}Pb was determined from its 46.5 KeV gamma emission, and ^{234}Th from its 63.3 peak (crosschecked with 92.3 KeV peaks). Concerning radionuclides from the ^{232}Th series, ^{228}Ra was estimated through ^{228}Ac (assessed as the average values from its 338 and 911 keV emissions), while ^{228}Th was evaluated as an average of ^{212}Pb (from its 238.6 KeV peak), ^{212}Bi (at 727.3 keV) and ^{208}Tl (583.2 and 2614.5 keV). Finally ^{40}K was measured via 1460.8 keV, and the anthropogenic ^{137}Cs by using its 661.3 keV gamma line.

Quality Control checks were performed through routine participation in National (Spanish Nuclear Safety Council, CSN) and International (IAEA and European Commission at JRC) Proficiency Tests.

2.4. Multielemental analysis by ICP-MS

For this study we use a sub-set of the analytes determined by ICP-MS in the work by Klubi et al. (2018), so for the full methodological details the reader is addressed to the above paper and to those by Enamorado-Báez et al. (2013, 2015). For self-consistency, it is worth mentioning that the US-EPA 3051A methodology for pseudo-total digestion was applied to aliquots of dried and homogenized sediment samples, including the use of H_2O_2 for enhancing organic matter mineralization.

For the present work we selected those elements informed in the used IAEA-405 reference material (exception of Hg – not quantified, Se – under MDL in most of the samples, and V – because of its low recovery with the pseudo-total acid digestion method), namely: Al, Cr, Mn, Fe, Co, Ni, Cu, Zn, As, Sr, Cd, Sb, Cs, Pb, Th and U.

2.5. Data treatment and statistical analysis

Statistical analysis was performed by using Statgraphics Centurion XVI.II software. After Kolmogorov-Smirnov (K–S) normality tests, we performed ANOVA and post-hoc mean comparison by Least Significant Difference (LSD) tests at 95% confidence level (CL) to assess differences between estuaries, and multivariate analysis for computation of the correlation matrices.

3. Results and discussion

3.1. Results description and LSD tests for means by estuary

The measured activity concentrations of radionuclides (^{40}K, ^{137}Cs, ^{210}Pb, ^{226}Ra, ^{228}Ra, ^{228}Th and ^{234}Th), along with the LOI and mud (fine fraction) contents in the sediment samples, are reported in Tables S1a–S1c (in electronic supplementary material, ESM) for the Ankobra, Pra and Volta estuaries, respectively. Lead-210 activity concentrations are contributed by two fractions, labelled as supported (from the in situ radioactive decay of ^{226}Ra) and unsupported ($^{210}Pb_{exc}$, from the radioactive decay of ^{222}Rn in the atmosphere). Table S2 (ESM) reports data from the multielemental analysis by ICP-MS.

The values of the analytes were normally distributed within each estuary. More precisely, they passed the K–S normality test, but $\log(x)$ transformations were necessary for LOI, Mn, Co and Cd in the Volta Estuary, for Sr and Cd in the Pra, and for Co in the Ankobra. In this last estuary the fine fraction (mud) required a $\sqrt{x}$ transformation. Table 1 reports a statistical summary for radionuclides, isotopic ratios and the

LOI and mud contents. For ICP-MS analytes a similar study can be found in Klubi et al. (2018). The analytical errors associated to the measurement of some radionuclides may not be negligible when compared against the dispersion of the measured values within each estuary, so they have been combined for the absolute uncertainty of each data. As the resulting uncertainties were non-uniform Table 1 reports the weighted means and their associated error (Gil and Rodríguez, 2001; Bevington and Robinson, 2003). Classes according to the Fisher's LSD test at 95% CL are also reported. This test is for the comparison of means for multiple samples, and different classes denote statistically significant differences at 95% CL. They follow the notation a, b, c from higher to lower values.

Sediments were overall sandy, but with large spatial variability in their mud content. The organic matter content (LOI_{440}) had mean values of 3.4%, 4.3% and 3.1% for the Ankobra, Pra and Volta estuaries, respectively (Table 1).

Potasium-40 activity concentrations were in the range of values reported in scientific literature for estuarine environments (e.g., Laissaoui et al., 2013; Klubi et al., 2017) with a mean value significantly higher in the Ankobra Estuary (after a Fisher's LSD test, Table 1).

The mean concentrations of ^{210}Pb were similar in the three estuaries, but those of $^{210}Pb_{exc}$ were significantly lower in the Ankobra and Pra estuaries (Table 1). Overall, their order of magnitude compares well with those reported by Klubi et al. (2017) for sediment cores from the Pra and Volta estuaries. Nevertheless, they show large spatial variability (as inferred from Tables S1a–S1c), particularly in the Volta Estuary, where their activity concentrations range from about zero up to 100 Bq/kg.

Owing to the elapsed time of several months since sampling to the γ-measurements, ^{234}Th (half-live 24.1 days) was in secular equilibrium with its parent radionuclide, ^{238}U. Their concentrations (Tables S1 and 1) compare well with the reference value of 35 Bq/kg reported by Viers et al. (2009) for sediments in African rivers. The mean values of concentrations for the measured radionuclides from the ^{238}U and ^{232}Th series are higher in the Pra estuary (Table 1), but at this stage it is not possible to elucidate whether this obey to different lithological fingerprints or to potential effects of gold-mining activities.

The ^{234}Th (^{238}U)/^{226}Ra ratio was of 1.13 ± 0.12 (mean and 1σ standard deviation of mean) in the Volta Estuary, similar to the value of 1.25 ± 0.11 found in the Pra Estuary, but in the Ankobra Estuary a statistically significant (at 95% CL) lower value was found: 0.79 ± 0.06. The above estimates are affected by both large uncertainties and large spatial variability, but secular disequilibrium is patent in the Ankobra Estuary.

In the continental Earth's crust the ratio between mean activity concentrations of ^{232}Th and ^{238}U is about unity. ^{228}Ra is the decay product of ^{232}Th, and in the Ankobra and Volta estuaries the ratio ^{234}Th/^{238}U)/^{228}Ra takes similar values (Table 1) which are close to the above reference, but it is significantly higher in the Pra Estuary. In all the samples, and taking into account the analytical uncertainties, ^{228}Th (half-live 1.9 y) was found in secular equilibrium with its parent radionuclide ^{228}Ra.

The ratio ^{226}Ra/^{228}Ra was also close to unity in the Pra and Volta estuaries (Table 1), but it was significantly higher in the Ankobra Estuary. This result, along with the above mentioned anomalous low ^{234}Th/^{226}Ra ratio suggests some enrichment of ^{226}Ra in the surficial sediments of the Ankobra Estuary. This effect has been reported in some estuarine and lacustrine environments and linked to groundwater discharges (e.g., Brenner et al., 2006). In this case, as there is a lack of independent evidences, the reasons for this anomalous isotopic ratio remain unknown.

Caesium-137 was under the minimum detectable activity (MDA) in most of the cases (Table S1). When quantified (at four sampling sites in the Volta, and one site in the Pra estuaries), concentrations were below 2 Bq/kg. These results compare well with those reported by Klubi et al. (2017) for sediment cores from two of these estuaries, and they are congruent with the known low atmospheric fallout rates of ^{137}Cs at these geographical latitudes (Hancock et al., 2011).

3.2. Gamma spectrometry versus ICP-MS

As above commented, ^{234}Th provides the ^{238}U content in the samples. This last isotope is also determined by ICP-MS (99.27% of isotopic abundance), but it is worth noting that the US-EPA 3051A method gets a pseudo-total acid digestion, leaving a varying and unknown refractory phase. ^{232}Th is quantified by ICP-MS (99.98% isotopic abundance), and γ-analyses provide activity concentrations for its daughter radionuclide ^{228}Ra, although secular equilibrium cannot be ensured under environmental conditions.

Fig. S1 (in ESM) plots the ^{234}Th (by γ) versus ^{238}U (by ICP-MS) and ^{228}Ra (by γ) versus ^{232}Th (by ICP-MS) for the three estuaries. While typical relative standard deviations were under 2% for ICP-MS analysis, they were of 20% in average for ^{234}Th determinations, and of 9% for ^{228}Ra. Both plots in Fig. S1 show high dispersion, although with statistically significant correlations for Ankobra and Pra estuaries. The agreement is poor, what is attributable to varying acid-digestion yields in the ICP-MS analysis and to poor representativeness of small size aliquots (~0.25 g). The case of Volta, where the higher discrepancies were revealed, will be discussed further below, on the light of subsequent analyses for this dataset (Section 3.3).

For the ^{234}Th vs ^{238}U plots, slopes are compatible with the unity, but they take lower values in the ^{228}Ra vs ^{232}Th plots (with statistical significance for Ankobra). A possible physical meaning is that ^{228}Ra is partially depleted in these sediments. This is a known phenomenon in

Table 1
Radionuclide activity concentrations, isotopic ratios, mud and LOI contents by estuary (weighted mean and associated errors– from datasets in Tables S1a, S1b and S1c).

	Ankobra Estuary			Pra Estuary			Volta Estuary		
^{40}K (Bq/kg)	377	±	35 (a)	321	±	20 (ab)	287	±	12 (b)
^{210}Pb (Bq/kg)	46	±	3 (a)	52	±	5 (a)	57	±	9 (a)
^{226}Ra (Bq/kg)	28.8	±	1.9 (a)	28.0	±	2.2 (a)	17.8	±	1.5 (b)
$^{210}Pb_{exc}$ (Bq/kg)	17.3	±	2.0 (b)	24	±	4 (b)	39	±	8 (a)
^{228}Ra (Bq/kg)	20.7	±	1.5 (b)	26.6	±	2.5 (a)	17.6	±	1.6 (b)
^{228}Th (Bq/kg)	23.0	±	2.0 (ab)	28	±	3 (a)	17.2	±	1.7 (b)
^{234}Th (Bq/kg)	22.3	±	2.0 (b)	32.3	±	2.6 (a)	20.5	±	2.5 (b)
^{234}Th/^{226}Ra	0.79	±	0.06 (b)	1.25	±	0.11 (a)	1.13	±	0.12 (a)
^{226}Ra/^{228}Ra	1.38	±	0.05 (a)	1.08	±	0.06 (b)	1.00	±	0.05 (b)
^{234}Th/^{228}Ra	1.09	±	0.09 (b)	1.30	±	0.11 (a)	1.14	±	0.10 (b)
Mud (%)	20.6	±	2.5 (ab)	26	±	3 (a)	18.6	±	2.4 (b)
LOI (%)	3.4	±	0.4 (ab)	4.3	±	0.5 (a)	3.1	±	0.5 (b)

For radionuclides and isotopic ratios, with non-negligible analytical uncertainties versus dispersion, the weighted means and their associated errors are reported (Gil and Rodríguez, 2001; Bevington and Robinson, 2003).
Classes a,b,c (in brackets) according to the Fisher's LSD test at 95% confidence level.

estuarine sediments (e.g., Veeh et al., 1995). Following the radioactive decay of ^{232}Th in the grain solids of the sediment, a fraction of the recoil ^{228}Ra atoms enter into the aqueous pore space and eventually reach the overlaying water column.

When plotting ^{238}U vs ^{232}Th, both measured by ICP-MS and expressed in units of Bq/kg, the slopes were of 0.56 ± 0.02, 0.43 ± 0.16 and 0.511 ± 0.15 for the Ankobra, Pra and Volta estuaries, respectively. This implies that while in the bulk sediment the isotopic activity ratio ^{238}U/^{228}Ra is slightly over the unity (Table 1), it is about the half for ^{238}U/^{232}Th in the acid-leachable phase. This suggests that most of the ^{232}Th is present in the acid-leachable phase, while only about half of the ^{238}U is found in this phase.

3.3. *Correlation matrices and inter-estuaries comparison of elemental associations*

This section is devoted to identify those metals and/or radionuclides which can represent some level of pollution and to delimit their potential sources.

The use of the geo-accumulation index (I_{geo}) and the enrichment factors (*EF*) for the set of ICP-MS determined analytes has been presented elsewhere (Klubi et al., 2018). The definition and a comprehensive analysis of these indexes can be found, among others, in Loring and Rantala (1992). When using the Volta Estuary as a reference background and Fe as normalizing element, values of *EF* over 2.0 were found for As, Sb, Cu, Cs and Cr in the Ankobra Estuary (the highest *EF* was 6.4 for As), and the same in the Pra Estuary, but for Sb and Cr (the highest *EF* was 2.75 for Cu), which is a moderate to significant enrichment (Klubi et al., 2018). When using Al as normalizing element, the *EF* for Cs was below 2.0 in both estuaries, indicating that Cs co-occurs with Al-silicates. When applied to the studied γ-emitter radionuclides, none of these indexes alert on enrichments in the Pra and Ankobra estuaries.

Tables S3a, S3b and S3c (in ESM) report the Pearson correlation coefficient matrices for the whole set of analytes included in this study, and for the three estuaries. They can be seen as a first-level of understanding on metal associations, providing some insights on their provenance.

One can distinguish two groups of analytes: i) the group of metals determined after pseudo-total acid digestion, and ii) the group including radionuclides and the physical characterization of the sediments (mud and LOI contents). Metals are measured in the acid-leachable fraction of the sediments (but concentrations are referred to the bulk mass), while radionuclide concentrations can be contributed by their whole mass. The three estuaries show different degrees of correlation among these two groups of analytes. It could be thought that the high correlation level observed among metals, particularly in the Ankobra Estuary, would be mediated by the pseudo-total acid-digestion method. Nevertheless, an also high correlation is observed among metals and radionuclides, particularly ^{40}K, what discards any artefact by the digestion method. The enriched metals show a high degree of correlation among them except for Sb in Ankobra, what is compatible with a common source. Nevertheless correlations are also high with many other elements, and from Tables S3a and S3b it is only possible discarding relevant particle-size effects and associations with Mn.

Additional insights on the origin of metal pollution and its potential association with radionuclides can be obtained by analysing the slopes in the linear correlations of the studied elements with Al, Fe and Cs. According to Loring and Rantala (1992), Al is a chemical tracer of Al-silicates, particularly the clay minerals, and it can account for granular variations of metal-rich fine silt and clay size Al-silicates. Iron (Fe) is a chemical tracer for Fe-rich clay minerals and hydrous Fe oxides. Caesium (Cs) is structurally combined in clay minerals and feldspars, and it is a tracer of clay minerals which are concentrators of trace metals.

In the present work the above tracer qualities must be understood within the scope of the adopted pseudo-total acid digestion. This is, as the content of the refractory phase does not account, the Al concentration (when referred to the bulk sediment mass) would be governed by the digestion yield and the varying amount of Al-silicates. If the leachable fraction was of uniform multielemental composition, the bulk concentration of all the elements would be linearly correlated with that of Al, with null intercepts at the origin. Different multielemental compositions in each estuary would reflect differences in slopes. The same apply when using Fe and Cs as a reference.

This is illustrated in Fig. 2, which plots Cr and As concentrations versus the Fe content in the three estuaries. Different slopes indicate different physic-chemical associations, and ordinates in origin significantly different from zero indicate, when positive, the presence of the analyte in other carriers with little or null Fe content, and, when negative, Fe can be found without measurable traces of the analyte.

Table 2 summarises the slopes for a group of metals when plotted versus Al, Fe and Cs (not included Co -with similar behaviour to Ni, Mn and Sr -with higher concentrations in the Volta, and Cd and Sb -with relatively low concentrations). The group of elements Cr, Ni, Cu, Zn, As and Cs showed a higher degree of association (properly higher slopes) with Fe in the Pra and Ankobra estuaries. A similar enhanced association with Al is observed in both estuaries only for Cr, Zn and As.

The Ankobra Estuary has relatively high concentrations of Al, Fe and Cs (Table S2), and the overall highest slopes (Table 2). This results in high metal extractions in the acid-leachable fraction and in strong correlations with the gamma-emitter radionuclides (Table S3a). The Volta Estuary has lower concentrations (by a factor 2–3) of Al, Fe and Cs (Table S2) than the other estuaries, and overall low Al and Fe-based

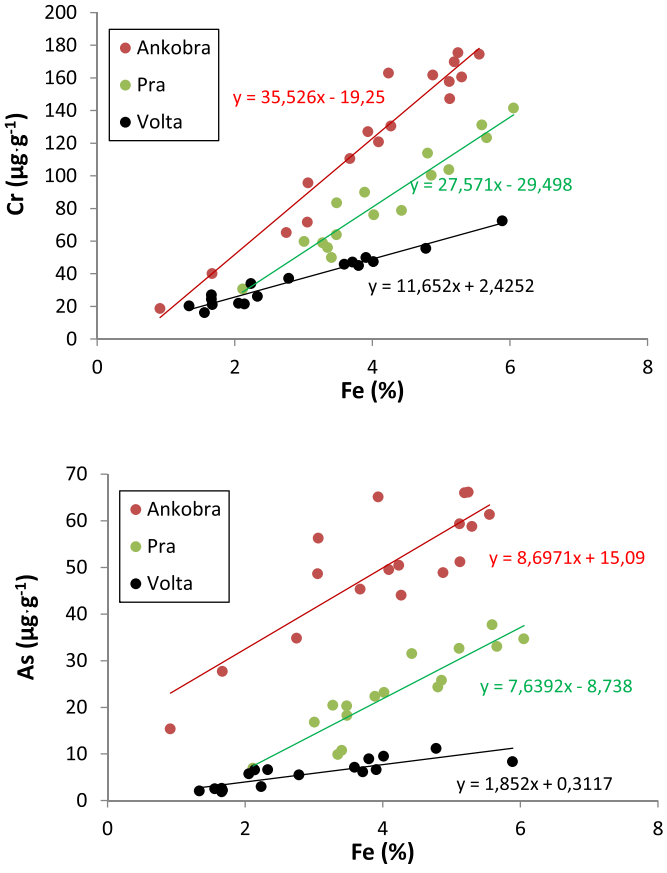

Fig. 2. Linear regressions for Cr and As versus Fe in sediments from the Ankobra, Pra and Volta estuaries. [$y = a+bx$; Cr vs Fe plot: a = −19 ± 9, b = 35.5 ± 2.2, $r = 0.97$, $p = 0.0000$ for Ankobra; a = −30 ± 9, b = 27.6 ± 2.2, $r = 0.96$, $p = 0.0000$ for Pra; a = 2.5 ± 2.1, b = 11.6 ± 0.7, $r = 0.98$, $p = 0.0000$ for Volta. Al vs Fe plot: a = 15 ± 6, b = 8.7 ± 1.4, $r = 0.84$, $p = 0.0000$ for Ankobra; a = −9±4, b = 7.6 ± 0.9, $r = 0.91$, $p = 0.0000$ for Pra; a = 0.3 ± 1.0, b = 1.8 ± 0.3, $r = 0.84$, $p = 0.0000$ for Volta – non-weighted fits].

Table 2
Slopes and standard errors for the linear regression of the selected trace elements versus Fe, Al and Cs contents, by estuary.

Element	Ankobra Estuary (n = 17)			Pra Estuary (n = 16)			Volta Estuary (n = 17)		
Linear regressions vs Fe									
Al (g/g)	2.48	±	0.14 **(b)**	3.2	±	0.5 **(a)**	2.06	±	0.16 **(b)**
Cr (mg/g)	3.55	±	0.22 (a)	2.76	±	0.22 **(b)**	1.16	±	0.07 (c)
Ni (mg/g)	0.664	±	0.025 (a)	0.70	±	0.06 **(a)**	0.48	±	0.04 (b)
Cu (mg/g)	0.641	±	0.025 (a)	0.61	±	0.06 (a)	0.31	±	0.03 **(b)**
Zn (mg/g)	1.21	±	0.05 (a)	1.11	±	0.12 (a)	0.80	±	0.03 **(b)**
As (mg/g)	0.87	±	0.14 **(a)**	0.76	±	0.09 **(a)**	0.19	±	0.03 (b)
Cs (mg/g)	0.075	±	0.003 **(b)**	0.084	±	0.006 **(a)**	0.044	±	0.004 **(c)**
Pb (mg/g)	0.270	±	0.005 (a)	0.286	±	0.027 (a)	0.267	±	0.013 **(a)**
Th (mg/g)	0.142	±	0.004 (a)	0.109	±	0.021 **(a)**	0.10	±	0.03 (a)
U (mg/g)	0.026	±	0.001 (ab)	0.018	±	0.008 **(b)**	0.035	±	0.005 (a)
Linear regressions vs Al									
Cr (mg/g)	1.42	±	0.06 (a)	0.75	±	0.06 **(b)**	0.54	±	0.04 **(c)**
Ni (mg/g)	0.261	±	0.011 **(a)**	0.191	±	0.015 **(c)**	0.232	±	0.007 **(b)**
Cu (mg/g)	0.247	±	0.017 **(a)**	0.146	±	0.026 **(b)**	0.149	±	0.008 (b)
Zn (mg/g)	0.47	±	0.03 **(a)**	0.27	±	0.05 **(b)**	0.365	±	0.023 **(c)**
As (mg/g)	0.33	±	0.06 **(a)**	0.18	±	0.03 **(b)**	0.080	±	0.017 **(c)**
Cs (μg/g)	29.6	±	1.2 (a)	21.5	±	2.6 **(b)**	21.3	±	0.6 **(b)**
Pb (μg/g)	105	±	5 **(b)**	73	±	10 **(c)**	123	±	7 **(a)**
Th (μg/g)	55	±	3 **(a)**	29	±	6 **(b)**	49	±	1 **(a)**
U (μg/g)	10.1	±	0.7 **(b)**	2.6	±	2.3 **(c)**	17	±	2 **(a)**
Linear regressions vs Cs									
Cr (g/g)	47.2	±	2.5 (a)	32	±	2 (b)	25.0	±	1.7 **(c)**
Ni (g/g)	8.8	±	0.3 **(b)**	8.3	±	0.4 (b)	10.8	±	0.3 **(a)**
Cu (g/g)	8.4	±	0.4 **(a)**	7.0	±	0.7 **(b)**	7.1	±	0.2 **(b)**
Zn (g/g)	16.0	±	0.7 **(a)**	13.1	±	1.1 **(b)**	17.0	±	1.2 **(a)**
As (g/g)	10.9	±	2.1 **(a)**	8.6	±	1.1 (a)	3.5	±	0.8 **(b)**
Pb (g/g)	3.54	±	0.11 **(b)**	3.40	±	0.21 **(b)**	5.7	±	0.4 **(a)**
Th (g/g)	1.86	±	0.07 **(ab)**	1.32	±	0.22 **(b)**	2.2	±	0.7 **(a)**
U (g/g)	0.34	±	0.02 **(b)**	0.20	±	0.09 **(b)**	0.83	±	0.08 **(a)**

Units for slope in brackets after the symbol of the element.
Classes a,b,c (in brackets) according to the Fisher's LSD test at 95% confidence level; when in boldface, they indicate that the intercepts at the origin are different from zero at 95% confidence level.

slopes for most of the tracers (Table 2), exception of the group Pb, Th and U. This enhances the differences with the group of analytes also determined in the refractory phase (i.e., the γ-emitter radionuclides), and explains the lack of correlation between both groups (Table S3c). The high discrepancy found in the Volta for the inter-comparison of γ and ICP-MS analyses can be then partially explained by the low metal content in the acid-leachable phase. This, in a large group of sandy samples in the Volta, also leads to poor and varying digestion yields. An also poor representability of the small-mass samples used for ICP-MS analysis cannot be discarded.

In Table 2 most of the intercepts at the origin were not null at 95% CL (indicated with classes in boldface), particularly for the linear regressions vs Al and Cs. This reveals other associations of the studied metals different from the Al-silicates and Cs-rich clay minerals. These associations can be better studied by using Al-normalized concentrations, to overcome the effect of varying digestions yields and the amount of Al-silicates, as shown in Fig. 3 ($X_{Al,N}$ = X/Al; where X and Al are the concentrations of the studied element and Al in the sample).

The Al-normalized concentrations of Ni and Pb increased with those from Fe following a similar pattern in the three estuaries (Fig. 3). The same was found for Al-normalized concentrations of ^{234}Th, ^{228}Ra, ^{226}Ra and ^{40}K. The Al-normalized concentrations of Cu, Zn, Cr and As were higher in the two estuaries with gold-mining activities, with similar values and behaviour for Cu and Zn, but with noticeably higher values for Cr and As in the Ankobra Estuary (Fig. 3).

A similar analysis using plots vs Al-normalized Cs ($Cs_{Al,N}$) shows that all data in the Volta appear grouped in the region of low $Cs_{Al,N}$ values, with null or negative correlation (Fig. 4, only data for Cr and As are shown). Data from the Ankobra appear grouped in a narrow and central region of $Cs_{Al,N}$, and without correlation. Only in the Pra Estuary the above group of elements (Cr, Ni, Cu, Zn, As and Pb) follow a clear pattern of increase with increasing $Cs_{Al,N}$ (Fig. 4). It is worth noting that $Cs_{Al,N}$ was positively correlated with $Fe_{Al,N}$ in the Pra Estuary, negatively correlated in the Volta, and uncorrelated in the Ankobra (at 95% CL).

Consequently there may be different sources of Fe-rich compounds which occur in "excess" with respect to the mean value of the Fe/Al ratio in the acid-leachable fraction of the sediment. The metal enrichments observed in the Ankobra (As, Sb, Cu, Cr) and Pra (As, Cu) estuaries are likely associated to mining-tailing particles. This is consistent with sulphide ores, mainly arsenopyrite [FeAsS], also rich in some metals (Nude and FoliYidana, 2011).

Concerning the pathways, mining tailings would be likely transported along the river course and deposited in the estuary where they can be mixed with different amounts of other terrigenous inputs. An alternative pathway could be the transport of some metals in the dissolved phase and their ulterior scavenging by suspended particulate matter. This will be discussed in section 3.4 on the light of the spatial distribution of concentrations and the local sedimentary conditions inferred from $^{210}Pb_{exc}$.

Table S4 (in ESM) shows similar information than Table 2, but for LOI and γ-emitters versus ^{40}K. Overall, correlations are strong (Table S3), and in all the cases the highest slopes appear in the Volta Estuary, where the mean concentration of ^{40}K is significantly lower (Table 1).

3.4. $^{210}Pb_{exc}$

The absence of $^{210}Pb_{exc}$ may reflect net erosional sites or freshly deposited materials with negligible meteoric ^{210}Pb contents (as expected from fresh mining tailings and non-surficial soils). High $^{210}Pb_{exc}$ contents may reflect smooth depositional areas where sediments accumulate at low rates with efficient scavenging processes for meteoric ^{210}Pb. Due to its origin, $^{210}Pb_{exc}$ is adsorbed at the particle surfaces, so its concentrations are higher in small grain-size particles with large specific surface areas (Abril, 1998a, 1998b; Alonso-Hernández et al., 2006). But in a dynamic sedimentary scenario the concentration of $^{210}Pb_{exc}$ also

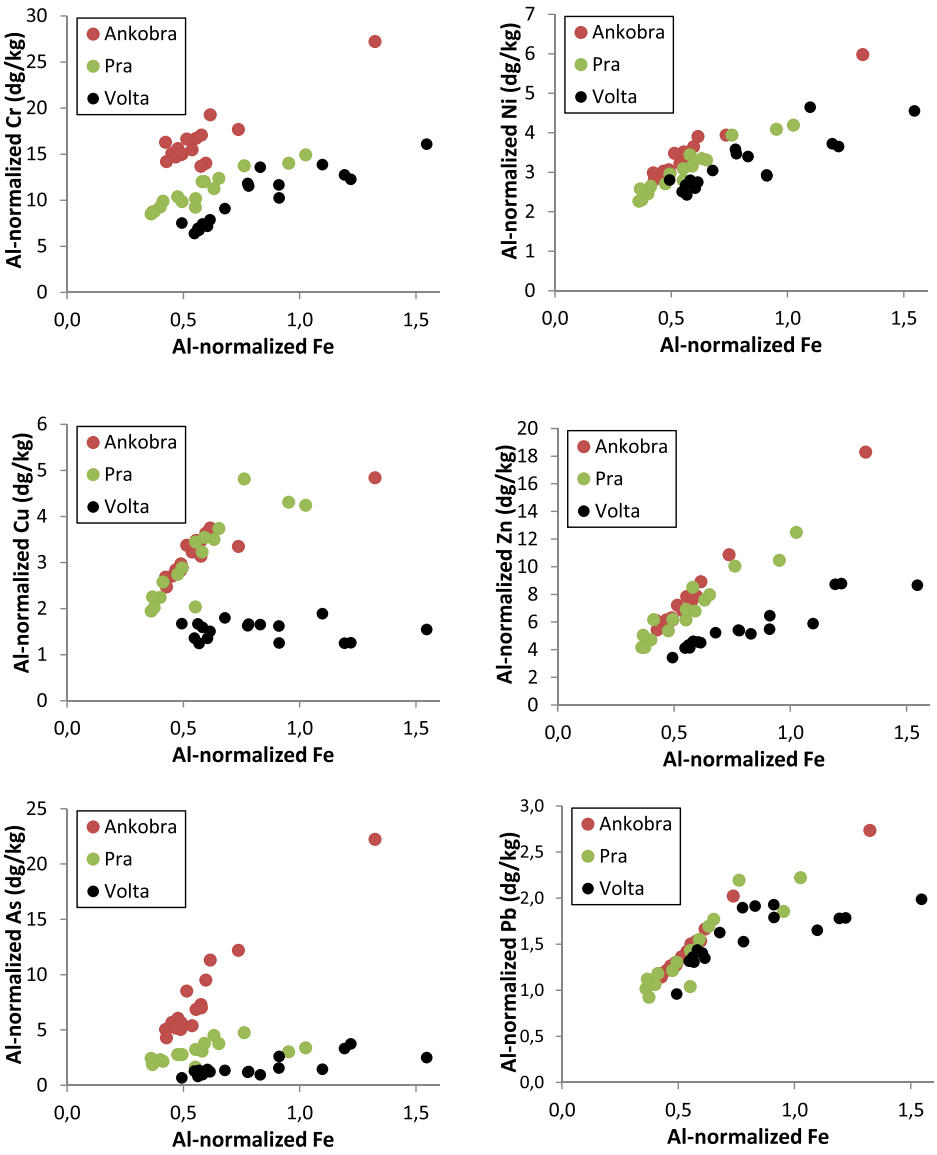

Fig. 3. Plots of Cr, Ni, Cu, Zn, As and Pb versus Fe in the three estuaries. All the concentrations have been normalized to the Al content. For an element with concentration X, is Al-normalized concentration is X divided by the concentration of Al in the same sediment sample. In the units, dg are 10^{-1}g.

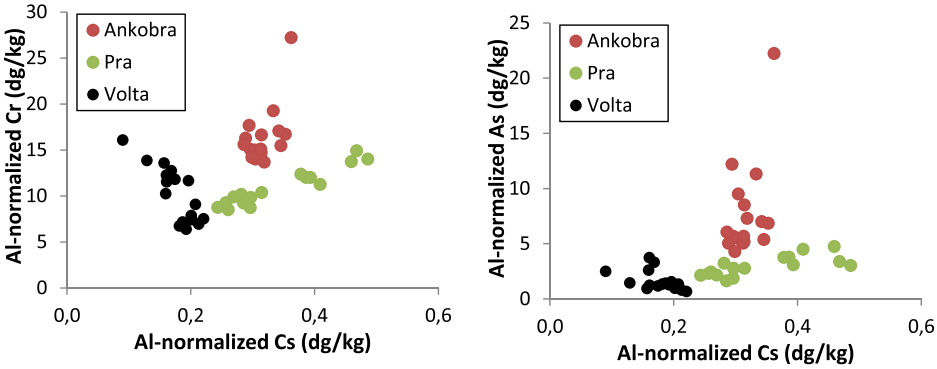

Fig. 4. As Fig. 3, but for Cr and As versus Cs, after normalizing all the concentrations to the Al content.

depends on the contact time, or time of opportunity for the uptake.

Fig. 5 tries to summarize the major features of spatial distributions of $^{210}Pb_{exc}$ and some metals (As, Cr, Pb and Fe, as potentially impacted by gold mining, and the last one also because its strong correlations with most of the metals - see Table S3, in ESM). Normalized (to their arithmetic means by estuary) concentrations are depicted versus sampling site (see Fig. 1). $^{210}Pb_{exc}$ data suggest a large diversity of local sedimentary conditions. For metals, high concentrations are found at most of

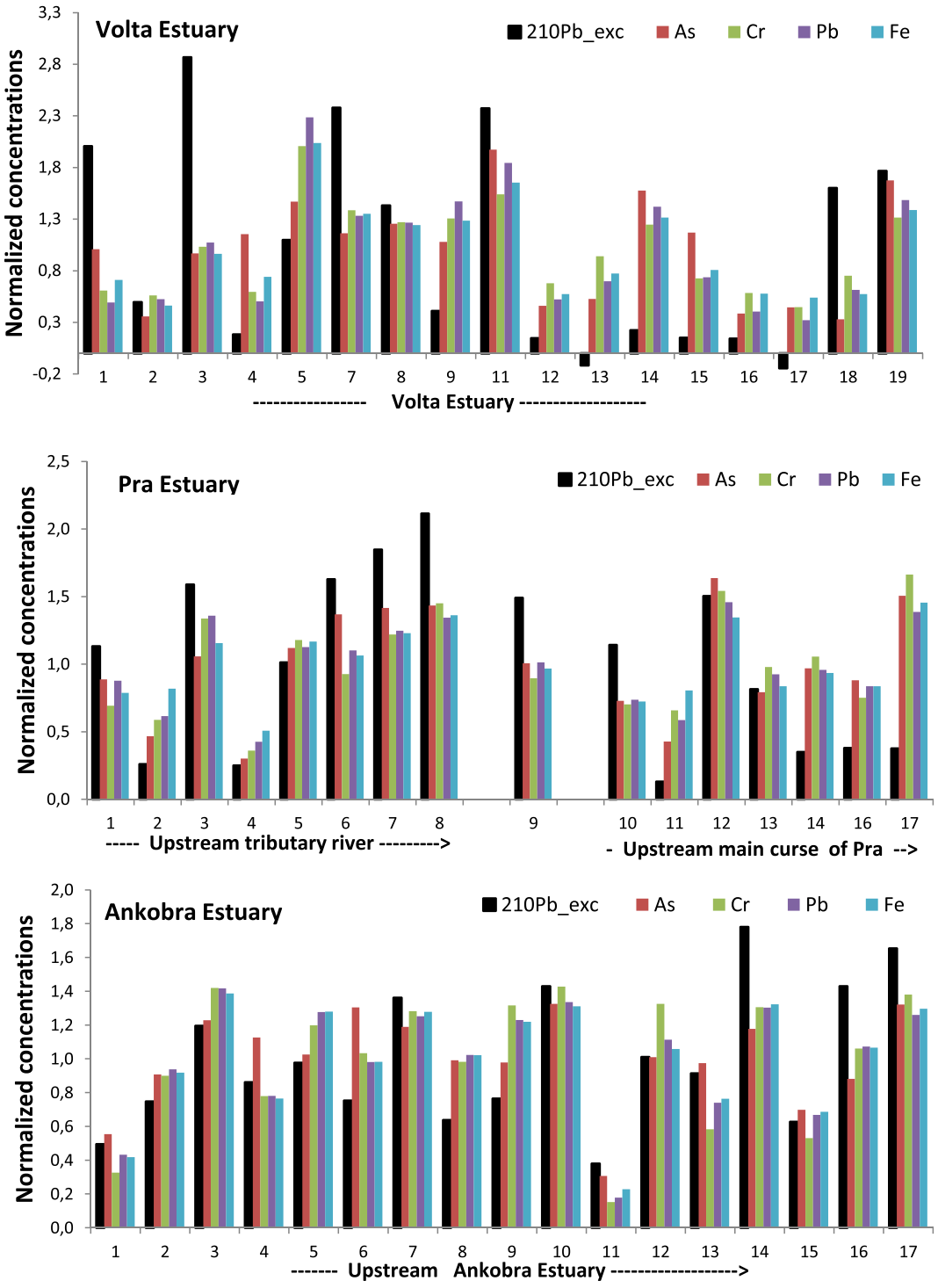

Fig. 5. Normalized (to their arithmetic means by estuary) concentrations of $^{210}Pb_{exc}$, As, Cr, Pb and Fe versus sampling site in the Volta, Pra and Ankobra estuaries (see Fig. 1).

the sampling sites, what seems consistent with non-localized sources for these elements.

In the Volta Estuary low $^{210}Pb_{exc}$ concentrations were found in sampling sites 12 to 17, around the island in the main channel of the Volta, where historical satellite photographs (Google Earth, Zoon Earth, satellites.pro and other websites) reveal the dynamic evolution of sand bars in the last three years. An also low $^{210}Pb_{exc}$ value appears at sampling site 2, where historical photographs reveal noticeable recoil of the shoreline. These dynamic sedimentary conditions involve the continuous and episodic reallocation (erosion/deposition) of large amounts of sediments whose metals content reflects the conditions at the sites and times of their provenance rather than recent local scavenging processes. Particularly, the above samples were mostly sandy (Table S1, in ESM) with an overall low metal content (Fig. 5). Smoother sedimentary conditions prevail in sites with high $^{210}Pb_{exc}$ concentrations, but this does not necessarily result in high metal concentrations (e.g., sites 3 and 7). Unlike the meteoric ^{210}Pb, which is scavenged from the water column by suspended particulate matter and surficial sediments, metals in the Volta Estuary must be mostly bound to solids since their provenances. Furthermore, the highest metal content appears in site 5, with moderate

$^{210}Pb_{exc}$ content, what can be likely attributable to local urban pollution.

From satellite images it is possible identifying the tidal limit of the Ankobra Estuary being about 8 km upstream from Asanta. The observed drastic changes in turbidity with the state of the tide suggest a strong dynamics of deposition and resuspension. This can enhance the time of opportunity for the uptake of meteoric ^{210}Pb. Nevertheless $^{210}Pb_{exc}$ concentrations in the Ankobra are lower than in the Volta (Table 1), what suggest that these concentrations are limited by the large amounts of suspended loads involved in the scavenging process. Satellite images also show the entry of some terrigenous inputs along the river banks, particularly in the river mouth. The concentrations of $^{210}Pb_{exc}$ show an overall trend of increase upstream within the sampling area. This trend is clearly interrupted at sampling points 11 and 15 (Fig. 5), the last likely affected by the on course works (at the time of sampling) for the construction of a new road north of Asanta, and the former being very sandy (2.2% mud, Table S1). $^{210}Pb_{exc}$ was also low around the urban area, in the river mouth. Under the above distinct sedimentary conditions the concentrations of the studied metals were also below their respective mean values. For the rest of the samples their concentrations were relatively uniform, with a relative standard deviation of 14% (Fig. 5). More properly, the correlation among $^{210}Pb_{exc}$ and most of the metals in the Ankobra Estuary (Table S3a) is mediated by the above points with low concentrations and abnormal sedimentary conditions. But for the rest, the concentrations of metals asymptotically tend to a constant value (Fig. 6). This result discards the scavenging from the dissolved phase as the dominant pathway for the observed enrichment in some metals.

In the Pra, historical satellite images show very high turbidity within the estuary. High $^{210}Pb_{exc}$ concentrations overall increased upstream along the explored tributary (Fig. 5) except for points 2 and 4 which were more sandy (Table S1). At these points, the studied metals were also below their respective mean values; while for the rest of the samples along the tributary their concentrations were relatively uniform (Fig. 5). Upstream the tributary, in the main course of the Pra, $^{210}Pb_{exc}$ concentrations were unexpectedly low despite the high mud content of the samples (Table S1) and while the metals concentrations kept relatively high values. This is compatible with meteoric ^{210}Pb being scavenged by large amounts of suspended loads which already contain relatively uniform and high concentrations of metals, likely supplied by upstream gold-mining runoffs. The large amount of mass involved in the uptake would lead to low $^{210}Pb_{exc}$ concentrations. This seems to be the case since in December 2017 a land barrier grew up blocking the main course of the river. The rupture of the former coastal sandbar at the far right allowed the river finding out its way to the sea, as shown in Fig. 7.

From the above analysis it can be concluded that the $^{210}Pb_{exc}$ concentrations in surficial sediments can provide useful insights on the local sedimentary conditions, which in the studied estuaries ranged from smooth to extreme. They also support the view of transport of mining tailing particles as the main pathway for the observed enrichment of some metals in the Pra and Ankobra estuaries. More experience is needed before establishing quantitative criteria for excluding samples which may contain pollution fingerprints significantly different from the current conditions of interest.

4. Conclusions

The concentrations of γ-emitter radionuclides from the ^{238}U and ^{232}Th series and ^{40}K in the studied sediments were in the range of their background values in the Earth's crust, and the artificial ^{137}Cs was under the detection limit is almost all the samples. Thus, they do not pose any radiological concern. Present data do not support any conclusion on their potential enrichments due to gold-mining activities.

Th and U allowed for a comparison of ICP-MS and gamma analyses. This revealed varying acid-digestion yields and some weakness in the representability of small sediment aliquots. The comparison also revealed radioactive secular disequilibrium between ^{228}Ra and its parent radionuclide, ^{232}Th.

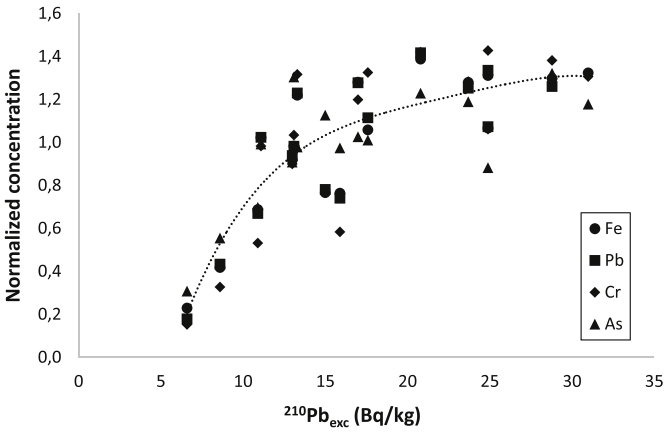

Fig. 6. Normalized concentrations (to their arithmetic means) of Fe, Pb, Cr and As versus $^{210}Pb_{exc}$ activity concentrations in the sediments from the Ankobra Estuary.

Fig. 7. Satellite image (from Google Earth) with the situation of the Pra Estuary on December 25th, 2017, after the formation of a sand barrier in the main course of the river and the breaching of the former coastal sand bar.

The metal enrichment observed in the Ankobra (As, Sb, Cu, Cr) and Pra (As, Cu) estuaries must be associated with forms of Fe-rich compounds with likely origin in mining-tailing particles, transported along the river course and deposited in the estuary. This is consistent with sulphide ores, mainly arsenopyrite [[FeAsS]. Mining tailings may be mixed with different amounts of other terrigenous inputs, so their fingerprint is weaker in the Pra estuary.

$^{210}Pb_{exc}$ and satellite images reveal large spatial and temporal variability in sedimentary conditions within each estuary, including sand bars dynamics, recoiling shorelines, and localized entries of terrigenous flows from the banks. Under smoother sedimentary conditions the concentrations of metals vs $^{210}Pb_{exc}$ show an asymptotic limit, what discards the scavenging from the dissolved phase as the dominant pathway for the observed enrichment. In the most upstream sampling sites in the Pra the uptake of meteoric ^{210}Pb is mediated by large amounts of suspended loads carrying the metals-fingerprint of gold mining tailings.

Declaration of competing interest

The authors declare no conflicts of interest.

Acknowledgments

The authors extend gratitude to the International Atomic Energy

Agency (IAEA) for supporting the Regional Project RAF7009 and the fellowship GHA-16025.

.

References

Abril, J.M., 1998a. Basic microscopic theory of the distribution, transfer and uptake kinetics of dissolved radionuclides by suspended particulate matter. Part I: theory development. J. Environ. Radioact. 41, 307–324.

Abril, J.M., 1998b. Basic microscopic theory of the distribution, transfer and uptake kinetics of dissolved radionuclides by suspended particulate matter. Part II: Applications. J. Environ. Radioact. 41, 325–342.

Abril, J.M., 2003. Difficulties in interpreting fast mixing in the radiometric dating of sediments using ^{210}Pb and ^{137}Cs. J. Paleolimnol. 30 (4), 407–414.

Abril, J.M., San Miguel, E.G., Ruiz-Cánovas, C., Casas-Ruiz, M., Bolívar, J.P., 2018. From floodplain to aquatic sediments: radiogeochronological fingerprints in a sediment core from the mining impacted Sancho Reservoir (SW Spain). Sci. Total Environ. 631–632, 866–878.

Alonso-Hernández, C.M., Diaz-Asencio, M., Muñoz-Caravaca, A., Delfanti, R., Papucci, C., Ferretti, O., Crovato, C., 2006. Recent changes in sedimentation regime in Cienfuegos Bay, Cuba, as inferred from ^{210}Pb and ^{137}Cs vertical profiles. Continent. Shelf Res. 26, 153–167.

Álvarez-Iglesias, P., Quintana, B., Rubio, B., Pérez-Arlucea, M., 2007. Sedimentation rates and trace metal input history in intertidal sediments from San Simón Bay (Ría de Vigo, NW Spain) derived from ^{210}Pb and ^{137}Cs chronology. J. Environ. Radioact. 98, 229–250.

Bempah, C.K., Ewusi, A., Obiri-Yeboah, S., Asabere, S.A., Mensah, F., Boateng, J., Voigt, H.-J., 2013. Distribution of arsenic and heavy metals from mine tailings dams at Obuasi Municipality of Ghana. Int. J. Engine Res. 2 (5), 61–70.

Bevington, P.A., Robinson, D.K., 2003. Data Reduction and Error Analysis for the Physical Sciences, third ed. McGraw-Hill, New York.

Botwe, B.O., Schirone, A., Delbono, I., Barsanti, M., Delfanti, R., Kelderman, P., Nyarko, E., Lens, P.N.L., 2017. Radioactivity concentrations and their radiological significance in sediments of the Tema Harbour (Greater Accra, Ghana). J. Radiat. Res. Appl. Sci. 10, 63–71.

Brenner, M., Whitmore, T.J., Riedinger-Whitmore, M.A., DeArmond, B., Leeper, D.A., Kenney, W.F., Curtis, J.H., Shumate, B., 2006. Geochemical and biological consequences of groundwater augmentation in lakes of west-central Florida (USA). J. Paleolimnol. 36, 371–383.

Costa-Böddeker, S., Thuyên, L.X., Hoelzmann, P., de Stigter, H.C., van Gaever, P., Huy, H.D., Schwalb, A., 2018. The hidden threat of heavy metal pollution in high sedimentation and highly dynamic environment: assessment of metal accumulation rates in the Thi Vai Estuary. Southern Vietnam. Environ. Pollut. 242, 348–356.

Donkor, A.K., Bonzongo, J.C., Nartey, V.K., Adotey, D.K., 2006. Mercury in different environmental compartments of the Pra river basin, Ghana. Sci. Total Environ. 368, 164–176.

Doyi, I., Oppon, O.C., Glover, E.T., Gbeddy, G., Kokroko, W., 2013. Assessment of occupational radiation exposure in underground artisanal gold mines in Tongo, Upper East Region of Ghana. J. Environ. Radioact. 126, 77–82.

Enamorado-Báez, S.M., Abril, J.M., Gómez-Guzmán, J.M., 2013. Determination of 25 trace element concentrations in biological reference materials by ICP-MS following different microwave-assisted acid digestion methods based on scaling masses of digested samples. ISRN Anal. Chem. 1–14 (Article ID 851713).

Enamorado-Báez, S.M., Gómez-Guzmán, Chamizo, E., Abril, J.M., 2015. Levels of 25 trace elements in high-volume air filter samples from Seville (2001−2002): sources, enrichment factors and temporal variations. Atmos. Res. 155, 118–129.

Fashola, M.O., Ngole-Jeme, V.M., Babalola, O.O., 2016. Heavy metal pollution from gold mines: environmental effects and bacterial strategies for resistance. Int. J. Environ. Res. Publ. Health 13, 1047–1067.

Gil, S., Rodríguez, E., 2001. Física Re-creativa, first ed. Pearson Education S.A, Perú (In Spanish).

Hancock, G.J., Leslie, C., Everett, S.E., Tims, S.G., Brunskill, G.J., Haese, R., 2011. Plutonium as a chronomarker in Australian and New Zealand sediments: a comparison with ^{137}Cs. J. Environ. Radioact. 102, 919–929.

Hierro, A., Bolívar, J.P., Vaca, F., Borrego, J., 2012. Behavior of natural radionuclides in surficial sediments from an estuary impacted by acid mine discharge and industrial effluents in Southwest Spain. J. Environ. Radioact. 110, 13–23.

Klubi, E., Abril, J.M., Nyarko, E., Laissaoui, A., Benmansour, M., 2017. Radioecological assessment and radiometric dating of sediment cores from dynamic sedimentary systems of Pra and Volta estuaries (Ghana) along the Equatorial Atlantic. J. Environ. Radioact. 178–179, 116–126.

Klubi, E., Abril Hernández, J.M., Nyarko, E., Delgado, A., 2018. Impact of gold-mining activity on trace elements enrichment in the West African estuaries: the case of Pra and Ankobra rivers with the Volta estuary (Ghana) as the reference. J. Geochem. Explor. 190, 229–244.

Koiter, a.J., Owens, P.N., Petticrew, E.L., Lobb, D.A., 2013. The behavioural characteristics of sediment properties and their implications for sediment fingerprinting as an approach for identifying sediment sources in river basins. Earth Sci. Rev. 125, 24–42.

Laissaoui, A., Mas, J.L., Hurtado, S., Ziad, N., Villa, M., Benmansour, M., 2013. Radionuclide activities and metal concentrations in sediments of the Sebou Estuary, NW Morocco, following a flooding event. Environ. Monit. Assess. 185, 5019–5029.

Larsson, C.M., 2008. An overview of the ERICA Integrated Approach to the assessment and management of environmental risks from ionising contaminants. J. Environ. Radioact. 99 (9), 1364–1370.

Loring, D.H., Rantala, R.T.T., 1992. Manual for the geochemical analyses of marine sediments and suspended particulate matter. Earth Sci. Rev. 32, 235–283.

Mabit, L., Benmansour, M., Abril, J.M., Walling, D.E., Meusburger, K., Iurian, A.R., Bernard, C., Tarjan, S., Owens, P.N., Blake, W.H., Alewell, C., 2014. Fallout ^{210}Pb as a soil and sediment tracer in catchment sediment budget investigations: a review. Earth Sci. Rev. 138, 335–351.

Macdonald, D.D., Carr, R.S., Calder, F.D., et al., 1996. Development and evaluation of sediment quality guidelines for Florida coastal waters. Ecotoxicology 5, 253–278.

Manjón, G., Mantero, J., Vioque, I., Díaz-Francés, I., Galván, J.A., Chakiri, S., Choukri, A., García-Tenorio, R., 2019. Natural radionuclides (NORM) in a Moroccan river affected by former conventional metal mining activities. J. Sustain. Min. 18, 45–51.

Mantero, J., Gazquez, M.J., Bolivar, J.P., García-Tenorio, R., Vaca, F., 2013. Radioactive characterization of the main materials involved in the titanium dioxide production process and their environmental radiological impact. J. Environ. Radioact. 120, 26–32.

Mauring, A., Gäfvert, T., 2013. Radon tightness of different sample sealing methods for gamma spectrometric measurements of 226Ra. Appl. Radiat. Isot. 81, 92–95.

Nude, P.M., Foli, G., Yidana, S.M., 2011. Geochemical assessment of impact of mine spoils on the quality of stream sediments within the Obuasi mines environment, Ghana. Int. J. Geosci. 2, 259–266.

Petersson, A., Scherstén, A., Gerdes, A., 2018. Extensive reworking of Archaean crust within the Birimian terrane in Ghana as revealed by combined zircon U-Pb and Lu-Hf isotopes. Geosci. Front. 9, 173–189.

Reese, A., Zimmermann, T., Pröfrock, D., Irrgeher, J., 2019. Extreme spatial variation of Sr, Nd and Pb isotopic signatures and 48 element mass fractions in surface sediment of the Elbe River Estuary - suitable tracers for processes in dynamic environments? Sci. Total Environ. 668, 512–523.

Robbins, J.A., 1978. Geochemical and Geophysical applications of radioactive lead isotopes. In: Nriago, J.P. (Ed.), Biochemistry of Lead in the Environment. Elsevier, Amsterdam, pp. 285–393.

Robbins, J.A., Edgington, D.N., 1975. Determination of recent sedimentation rates in Lake Michigan using ^{210}Pb and ^{137}Cs. Geochem. Cosmochim. Acta 39, 285–304.

Sánchez, C.I., García-Tenorio, R., García-León, M., Abril, J.M., El-Daoushy, F., 1992. The use of ^{137}Cs in marine and lacustrine sediment dating. Nucl. Geophys. 6 (3), 395–403.

Sun, X., Fan, D., Liu, M., Liao, H., Tian, Y., 2019. Persistent impact of human activities on trace metals in the Yangtze River Estuary and the East China Sea: evidence from sedimentary records of the last 60 years. Sci. Total Environ. 654, 878–889.

Tarazona, J.V., Versonnen, B., Janssen, C., De Laender, F., Vangheluwe, M., Knight, D., 2014. Principles for Environmental Risk Assessment of the Sediment Compartment: Proceedings of the Topical Scientific Workshop. European Chemicals Agency. ECHA-14-R-13-EN.

Travesi, A., Gascó, C., Pozuelo, M., Palomares, J., García, M.R., Pérez del Villar, L., 1997. In: Desmet, et al. (Eds.), Distribution of natural radioactivity within an estuary affected by releases from the phosphate industry. Freshwater und Estuarine Radioecology. Elsevier Science B.V., pp. 267–279

Veeh, H.H., Moore, W.S., Smith, S.V., 1995. The behaviour of uranium and radium in an inverse estuary. Continent. Shelf Res. 15 (13), 1569–1583.

Viers, J., Bernard Dupré, B., Gaillardet, J., 2009. Chemical composition of suspended sediments in World Rivers: new insights from a new database. Sci. Total Environ. 407, 853–868.

Villa, M., Manjón, G., Hurtado, S., García-Tenorio, R., 2011. Uranium pollution in an estuary affected by pyrite acid mine drainage and releases of naturally occurring radioactive materials. Mar. Pollut. Bull. 62, 1521–1529.

Winde, F., Sandham, L.A., 2004. Uranium pollution of South African streams – an overview of the situation in gold mining areas of the Witwatersrand. Geojournal 61, 131–149.